A98-31505

ICAS-98-2,4,4

UNSTEADY TRANSONIC HYBRID INTEGRAL-EQUATION/ FINITE-VOLUME SCHEME FOR TRAJECTORY SIMULATION OF STORES WITH TIME-STEP ADAPTATION

Arya K. Bhattacharya
Aeronautical Development Agency, Bangalore, India
V. Kanagarajan
National Aerospace Laboratories, Bangalore
S.R. Mohan
Aeronautical Development Agency, Bangalore

Abstract

Development of a simulation program AMAR to predict the state-histories of stores released from fighter aircraft is described in this paper. AMAR computes configuration aerodynamics using a coupled integral-equation finite-volume scheme to solve the unsteady full-potential equation. This scheme discretizes the problem using surface panels embedded in a configuration-independent rectangular field grid - an approach that 'naturally' facilitates solution of flow over configurations with components in relative motion, as typical of the separating store problem. Computed aerodynamics is accuracy-accretized by accounting for real-flow effects, through synthesis with a-priori test data on stores in freestream using concurrently developed concepts. Aerodynamic prediction techniques are synergized with store and aircraft flight dynamics in the AMAR code to simulate trajectories of arbitrary stores released from aircraft. Fuzzy logic control to optimize time step size Δt for maximum simulation accuracy in minimum computation time is implemented. Trajecto-ies obtained using steady-flow computations are compared against NAL 1.2m trisonic wind tunnel CTS simulations on fuel tanks released from fighter aircraft models at subsonic and transonic speeds. Finally the concept of 'artificial hysteresis' is introduced to isolate and measure unsteady effects on bodies executing non-oscillatory motion as typical of separating stores.

Introduction

Simulation of trajectory of stores released from aircraft plays an important role in development and integration of fighter aircraft weapon systems. All the stores should be released such that they exit the aircraft aerodynamic-influence-zone clean - without contacting the aircraft or its components - and the store motion is not destabilized beyond recovery. The early trials towards clean separation are too risky to be undertaken directly in flight, and they have perforce to be simulated. Accurate simulation of trajectory within parent aircraft aerodynamic-influence-zone also has the potential to significantly cut down flight test efforts and cost.

Trajectory simulation of stores within aircraft aerodynamic influence zone is composed essentially of two components - aerodynamic predictions and numerical integration of equations of motion, with possible inputs from a third - aircraft and/or store guidance and control commands. Aerodynamic inputs to simulation may be generated either in a wind-tunnel (WT), completely from Computational Fluid Dynamics (CFD), or through a hybrid approach that optimally combines data from both these sources.

Wind tunnel data is preferable to the extent that it incorporates real-flow effects. However, there are certain limitations in use of WT data for store separation studies, relating primarily to the absence of dynamic effects. Also, generating an aerodynamic data-base for the store calls for a large number of independent parameters to be considered - both aircraft and store flight conditions and their relative positions. Aerodynamic data generated using CFD alone will be reliable only if real-flow effects that critically affect trajectory are accounted for. These include skin-friction drag, shock-induced separation effects at store boat-tail, and incidence induced separation at store leeward surfaces. An inviscid code, either full-potential or Euler, is inherently deficient in predicting all these quantities. In the case of incidence-induced leeward separation, the error is more consistent, though usually larger, for potential as compared to Euler solutions (see section on 'Data Synthesis'). Only NS solutions with an ability to accurately model transition and separation can be trusted to independently provide data of high fidelity.

Thus, a cost-effective approach that can generate high fidelity aerodynamic data seems to be an optimal fusion of unsteady full-potential predictions obtained in aircraft interference zones with limited WT test data, so that real flow- as well as dynamic- effects are captured accurately and efficiently. This forms the basis of the present method.

The unsteady full potential equation is solved using an integral equation to obtain potential distribution on configuration boundaries, followed by a finite volume solution in the field to obtain potentials as well as compressibility and 'time-lag' sources[1-3]. The configuration

surface is discretized using flat panels embedded in a surface-independent rectangular field grid. This arrangement easily handles moving components — the paneled moving surface simply cuts through the enveloping rectangular field grid, only the identity of surface-intersecting field cells change.

Accuracy accretization of computed inviscid aerodynamic coefficients to account for real flow effects is performed by synthesis with WT data on isolated store at large incidences, as also on store in carriage position. The corrections obtained at freestream are projected into interference zones using a concurrently evolved concept of 'accuracy-interference increment parallelogram', a variant of the principle of accuracy of incremental coefficients[4,5].

Trajectories obtained from the simulation program AMAR (astra marg pradarshak) with aerodynamics computed by steady flow equations compare reasonably against those obtained using WT Captive Trajectory System (CTS) for full and empty fuel tanks at subsonic and transonic speeds. Validation of predicted dynamic effects are not straightforward and need flight tests with appropriate data collection. In this context a new concept of 'artificial hysteresis' is evolved[6] to isolate and measure the unsteady effects and to check the necessary conditions for their correctness.

The time step size Δt used in a simulation needs to be optimized meeting conflicting requirements of maximizing solution accuracy (i.e. small Δt) and minimizing solution time (large Δt). In time-marching CFD codes stability requirements determine and restrict the choice of Δt, which is not a consideration in the Poisson-type solvers used in the present approach. Hence potential exists to adapt the size of Δt with factors like store aerodynamic stability, ratio of aerodynamic- to inertial- forces, and rates of change of aerodynamic coefficients with time. Accordingly fuzzy-logic based open loop control of Δt is implemented in AMAR.

The unsteady hybrid computational scheme is described below. The technique to unify CFD and test predictions to generate aerodynamic data of high fidelity is described next. Finally the results, especially in terms of simulated trajectories and their comparison against test, are presented.

Unsteady hybrid integral equation - finite volume scheme

Formulation

The unsteady full potential equation may be expressed in mass conservation form

$$\partial\rho/\partial t + \nabla.(\rho\nabla\Phi) = 0 \qquad (1)$$

with density

$$\rho = [1+ ((\gamma-1)/2)M_\infty^2\{1- (\nabla\Phi)^2 -2\partial\Phi/\partial t\}]^{1/(\gamma-1)} \qquad (2)$$

where Φ, ρ, γ and M denote potential, density, ratio of specific heats and Mach number.

When Eq.(1) is written in the form of a Poisson equation

$$\nabla^2\Phi = -[\nabla\rho.\nabla\Phi + \partial\rho/\partial t]/\rho \qquad (3)$$

the solution for potential may be expressed, from the theory of integral equations, as a sum of three integrals - two over the surface and one over the field, as

$$\phi(P)= \iint_S \sigma(Q)K_\sigma dS + \iint_S \mu(Q)K_\mu dS + \iiint_V G(Q)K_\sigma dV \qquad (4)$$

where S and V denote configuration surface and field domain, ϕ is the perturbation potential defined as $\phi = \Phi - \Phi_\infty$, and

$$K_\sigma = -1/4\pi r, \qquad K_\mu = \hat{n}.\nabla(-K_\sigma), \qquad \bar{r} = \bar{Q} - \bar{P} \qquad (5)$$

$$\sigma = \Delta(\hat{n}.\nabla\phi),\ \mu = \Delta\phi,\ G = -(\nabla\rho.\nabla\Phi)/\rho - (\partial\rho/\partial t)/\rho$$

Δ denotes jump across a surface. Further, on imposing the internal Dirichlet condition of zero disturbance potential within closed volumes, one obtains

$$\sigma = \partial\phi/\partial n \quad \text{and} \quad \mu = \phi \qquad (6)$$

It may be seen that nonlinear compressibility effects, as also unsteady effects, are both contained in the term 'G', the source term in the Poisson equation (3). G is composed of a steady and an unsteady component, $G = G_{steady} + G_{transient}$. Setting G=0 reduces the above scheme to the steady linear panel methods, while setting $G_{transient}=0$ gives the formulation for integral solution of steady full potential equation that forms the basis of the Field Integral Method (FIM) code[1-2].

Boundary conditions

The flow tangency boundary condition is implemented for steady flow by setting explicitly

$$\sigma = -\bar{V}_\infty.\hat{n} \qquad (7)$$

When the body-fixed reference frame (≡ computational frame) translates and rotates w.r.t. freestream in a transitory manner, freestream velocity V_∞ in computational frame varies in space-time and may be expressed as $\bar{V}_\infty = \bar{V}_\infty(t) + (\bar{\Omega}(t) \times \bar{r})$, where $\Omega(t)$ is angular velocity around fulcrum of rotation, r is distance of considered point from the fulcrum.

For the present store separation problem, the computational frame (i.e. the aircraft-body) is usually steady w.r.t. freestream while the store translates and rotates w.r.t. both. Accordingly the boundary condition on moving store becomes

$$\sigma = -(\bar{V}_\infty + \bar{V}'(t) + \bar{\Omega}(t) \times \bar{r}).\hat{n} \qquad (8)$$

where V' is relative translational velocity of store w.r.t. computational axes. For configuration components that are steady w.r.t computational axes, Eq.(7) holds good.

The far-field boundary condition of vanishing perturbation potentials is satisfied naturally by the scheme since the disturbance at any point varies inversely as its distance from the disturbing surface, as may be seen from Eqs. (4) and (5).

Field Solution

The potential equation (1) may be expressed as conservation of mass flux through surface S_C of a closed volume D_C in the fluid domain

$$\iint_{S_c} \rho \mathbf{n}.\nabla\Phi \, dS = -\iiint_{D_c} \partial\rho/\partial t \, dV \qquad (9)$$

This leads to the finite-volume formulation for evaluation of field potentials.

In supersonic regions of flow artificial viscosity is added, to account for change of equation type, by a mass-flux biasing approach for evaluating field sources, and a density biasing approach for computing the field potentials[1].

Numerical Procedure

The numerical evaluation of potential distribution on configuration surface is accomplished by solving a discretized form of Eq. (4). The potentials in the field are evaluated by a finite-volume procedure that follows from consideration of mass conservation across the closed surface of a cell, as expressed in Eq. (9). The field solution uses the computed surface potentials as a Dirichlet boundary condition.

The configuration surface is discretized into flat panels, with constant potential on a panel, and the paneled configuration is immersed in a rectangular field grid which in principle (with liberty towards flow- and geometry-feature adaptivity of grid) is independent of surface. The field grid serve as vertices of field cells, with constant potential in each cell.

Equation (4) may be written in a discretized form as

$$\phi_i = \sum_{j=1}^{N} \sigma_j B_{ij} + \sum_{\substack{j=1 \\ j\neq i}}^{N} \mu_j C_{ij} + \sum_{k=1}^{M} G_k D_{ik} \qquad i=1,N \qquad (10)$$

where N, M are total number of surface panels on configuration and cells in field, respectively; B_{ij}, C_{ij} and D_{ik} are influence coefficients from surface sources, surface doublets and field sources respectively to surface panel centroids, and are given as

$$B_{ij} = \iint_{\text{Panel } j} K_{\sigma_{ij}} dS; \quad C_{ij} = \iint_{\text{Panel } j} n_j \nabla_j(-K_{\sigma_{ij}}) dS; \quad D_{ik} = \iiint_{\text{Cell } k} K_{\sigma_{ik}} dV \qquad (11)$$

It follows from the internal Dirichlet formulation that $\phi_i = \mu_i$ for all surface panels i, thus Eq.(10) becomes

$$\sum_{j=1}^{N} \mu_j C_{ij} = \sum_{j=1}^{N} \sigma_j B_{ij} + \sum_{k=1}^{M} G_k D_{ik} \qquad (12)$$

σ_j are evaluated a-priori using Eqs. (7) and (8), G_k are evaluated using Eq. (5) and latest available values of field potentials ϕ and densities ρ, thus Eq. (12) constitutes a linear system for computing μ.

There are three types of field cells — those totally immersed in the body, those which intersect the surface, and those completely outside the body. Consistent with the internal Dirichlet formulation, field sources for the cells that lie completely inside are of zero strength. The cells that cut the surface acquire the value of potential held by the portion of the surface intersected by the cell. This is implemented through a bilinear interpolation — from four nearest surface panel centroids to field-cell centroid. The values obtained on the surface-intersecting cells are then used as Dirichlet boundary condition for computation of potentials in the cells lying completely in the field, using the finite-volume formulation presented below.

The finite volume scheme for computation of field potentials uses a discretized form of the mass conservation equation (9)

$$\sum_{i=1}^{6} W_i \rho_i \bar{V}_i \hat{n}_i = -D_0 \, \partial\rho_0/\partial t \qquad (13)$$

where i=1,6 represent six faces of a cuboidal cell, W_i is wall area of face i, V_i is the velocity at the face, and D_0, ρ_0 are volume and density in considered cell. Further,

$$\bar{V}_i.\hat{n}_i = (\phi_i - \phi_0)/d_i + \bar{V}_\infty \hat{n}_i \qquad (14)$$

where ϕ_0 is perturbation potential at cell centroid, ϕ_i is perturbation potential in centroid of cell lying across face i.

Substituting (14) in (13), it is possible to obtain a three-point implicit SLOR scheme as

$$-a_5\phi_5 + A\phi_0 - a_6\phi_6 = \sum_{i=1}^{4} a_i\phi_i + \sum_{i=1}^{6} b_i V_\infty n_i - D_0 \, \partial\rho_0/\partial t \qquad (15)$$

where $a_i = W_i\rho_i/d_i$, $b_i = W_i\rho_i$, $A = \sum_{i=1}^{6} a_i$,

$\partial\rho/\partial t$ is obtained by first-order backward time-differencing. Subscripts 5 and 6 denote the z- lower and upper faces of a cell. Equation (15) is solved implicitly in a z-column, and then by marching in the y- and x- directions, in that sequence. For each z-column the above equation forms a tridiagonal matrix that is solved using an efficient algorithm. The cell that intersects the boundary forms the first cell in each such z-column and generates the first row in the corresponding tridiagonal matrix, and its potential value obtained by interpolation from the surface 'feeds' the boundary condition into the implicit solution.

The field potentials obtained using above finite-volume scheme are used to obtain field densities using Eq. (2), and field sources 'G' using Eq. (5). The updated values of G are used in Eq. (12) to obtain surface potentials ϕ (=μ) at next iteration level. These updated potential values are then fed into the field using the finite-volume scheme, and this process continues till surface potentials converge.

Surface potentials are used to obtain pressure distribution which on integration gives required aerodynamic coefficients.

It is noteworthy that though the full-potential equation becomes hyperbolic on addition of unsteady time-derivative terms, its numerical solution in the form of a Poisson equation (Eq. (3) and its finite-volume derivatives) with the time-dependent terms encapsulated in the source at right, maintains structural similarity and hence identical convergence characteristics as the solution of steady full-potential equation. This implies that the time step size does not explicitly affect the stability of the schemes, a fact that underlies the development of time-step adaptation procedures described below.

Synthesis of computation and test data

Aerodynamic coefficients on store computed using the above integral equation - finite volume scheme (its steady version henceforth referred to as FIM code), and enhanced by corrected values of drag coefficient, can be considered sufficiently accurate for a first-cut prediction of trajectories. There are certain effects, however, that this computational model is unable to capture adequately, but which may influence trajectory evolution to some extent. They include the following —

i) for the store in carriage position on aircraft, a channel-like flow develops between wing lower surface, store upper surface and pylon, that may terminate near store boat-tail in strong shocks inducing boundary-layer (BL) separation on the store surface, with attendent influence on aerodynamic coefficients

ii) on a separating store that attains high incidence angles (e.g. empty fuel tank), flow separation occurs on leeward side on cylindrical portion of the store - leading to inadequate pressure recovery and consequent nonlinear increase in forces in plane normal to store axis.

Both the above effects cannot be correctly captured by any inviscid computations. This is applicable to Euler solutions as well, though under conditions where sharp features in configuration geometry induce flow separation, some of the above characteristics may be captured[6]. This ambivalent recovery of real flow features induces certain inconsistencies in the error (in terms of deviation between computed and real flows) obtained on an Euler solution, with corresponding uncertainties in corrective techniques to recover these effects. A potential solution, on the other hand, is consistently 'ignorant' of the separation features- with a corresponding ease of construction of corrective factors to account for real flow effects.

Wind tunnel tests on isolated store are able to capture the above-mentioned nonlinear increments at higher incidences, as observed in Figs. 2 and 3 for the fuel tank shown in Fig. 1. Figures 2 and 3 also show FIM results; good comparison between the computations and the tests at low incidences, and their deviation with increasing incidence due to larger nonlinear effects, are clearly visible. These comparisons led to the evolution of empirical relations[7] that bridge the deviation between FIM results and real flows, so that computed predictions on a similar class of store configurations at varying flight conditions may be mapped into real flow characteristics without recourse to further testing. The empirical relations are a function of, firstly, the computed FIM values, secondly, the incidence angle, and also the planform area of the store constant-section zone. It is seen from Figs. 2 and 3 that these empirical relations are able to adequately represent nonlinear effects.

The above synthesis of computational and experimental data is evolved at freestream conditions of store. This can, further, be extended to regions of aircraft interference, on applying the principle of incremental coefficient accuracy and associated concept of 'accuracy-interference increment parallelogram' explained here. The principle of incremental coefficient accuracy[4,5] implies that absolute values of predicted aerodynamic coefficients on a store, in freestream and in regions of aircraft interference, may vary significantly with the method used for prediction, however, the incremental effects of aircraft interference will be quite close across the range of prediction methods. From this the 'accuracy-interference increment parallelogram' follows deductively. Figure 4 shows interference intensity on the x-axis and a generic aerodynamic coefficient on y-axis. A_{ij}, i=1,2, j=1,2, represent the coefficients obtained at interference level i from method j. From the incremental coefficient accuracy principle, the increment in coefficient due to interference predicted by method 1 $\cong$ increment due to interference from method 2, i.e. $A_{21} - A_{11} \cong A_{22} - A_{12}$, and the polygon $A_{11}A_{12}A_{22}A_{21}$ forms a parallelogram (opposite sides parallel and equal). It immediately follows that $A_{12} - A_{11} \cong A_{22} - A_{21}$, i.e. the increment due to methodological accuracy at interference level 1 is projected unmodified into interference level 2. On applying this concept to the present problem, the empirical relations used on FIM predictions to capture real flow effects at freestream conditions (representing increments due to accuracy at freestream), are extended to FIM predictions in interference zones for recovering the corresponding real-flow features.

The above empirical corrections on inviscid CFD solution to recover real-flow effects may be invalidated at/very-near carriage where coupling of store- and aircraft-induced disturbances lead to nonlinearities like shocks and resultant separations. Thus, to maintain consistency of accuracy levels, it is preferable to use aerodynamic coefficients at carriage position from WT source alone.

To summarize, aerodynamic data at carriage position is taken exclusively from WT tests to maintain high data fidelity levels. For all other store positions, steady/unsteady FIM solution refined by WT data through the incremental coefficient accuracy principle, is used for store aerodynamic predictions.

Trajectory Simulations

Predicted store aerodynamics is used as input in nonlinear 6-DOF equations of motion to simulate trajectories. The 6-DOF equations are numerically integrated to 4^{th}-order accuracy using a Runge-Kutta scheme at first time step and an Adams' multistep predictor-corrector technique at succeeding steps.

The fuel tank shown schematically in Fig.1 is released from an Indian fighter aircraft (IFA-1) under various aircraft flight- and fuel tank mass- conditions, and resulting separation trajectories are simulated. Results in terms of evolution of store states are presented for some representative cases, and computations are compared against the tests wherever possible. The comparisons are only for quasi-steady cases neglecting dynamic effects. Since the accuracy (or otherwise) of aerodynamic predictions constitute the major factor of uncertainty in simulation correctness, some comparisons are also presented between static-store computed aerodynamics and WT measurements. Further, the unsteady simulations are 'dissected' to isolate and analyze dynamic effects using a new approach that may be termed as 'artificial hysteresis'.

Dependence of store state histories on selected time step size 'Δt' are also investigated.

Pressure distributions on IFA-1 wing and fin mid-span sections at transonic Mach numbers (M) and low incidence (α) and sideslip (β) are obtained from FIM and compared against test data in Figs. 5 and 6. These comparisons serve to fortify a general confidence in FIM code for solution over complex configurations. Figures 7 and 8 compare FIM pressure distributions against measurements on two wing sections just in- and out- board of the pylon that carries the fuel-tank, at M=0.9. The presence of a shock corresponding to location of store boat tail is visible in both the tests and computations. Shock is formed due to termination of the expansion zone formed in the channel-like flow between wing lower surface, store upper surface and pylon. Reducing incidence angle leads to stronger shock formation caused by higher expansion of flow in the 'channel'. Figures 9-12 show variation of store aerodynamic coefficients C_N, C_m, C_S and C_n with aircraft incidence angle α, when store is in carriage position. FIM computations are compared against measurements. The deviation is quite small in the α-range 2°-5°, which coincides with operating α-range of flight typical of fuel-tank carriage. At lower α the deviation increases due to shock-induced flow separation on store, as evidenced by the large divergence in test values at the transonic Mach number as compared with test results at shock-free M=0.5, as also with the computations.

Wind Tunnel Captive Trajectory System

The most common ground-based experimental technique that can provide reliable test data for comparison of trajectory results for validation of theory is the Captive Trajectory Simulation (CTS) technique. Hence a few trajectory results were obtained on the store using the CTS system in the 1.2m trisonic Wind Tunnel of National Aerospace Laboratories (NAL).

Wind Tunnel:

Tests were carried out at the NAL wind tunnel. This facility is an intermittent blowdown tunnel with a test section size of 1.2m x 1.2m and a Mach number capability of 0.2 to 4.0. Tests at transonic speeds are conducted in a test section with perforated walls. The top and bottom walls have an open area ratio of 6% and the side walls have an open area ratio of 20%. Aircraft model is mounted on an internal strain gauge balance fixed at the end of a support sting. The sting in turn is held by a model support system which permits the model to be pitched to the desired angle.

NAL CTS System:

The NAL CTS has a 6-DOF mechanical rig, a control system and a computer system. The compact independent mechanical rig is driven by electro-mechanical drives to provide 6-DOF movements, and is floor mounted on the wind tunnel (Fig. 13). The store model is mounted on the CTS rig through a 6-component strain gauge balance to measure the loads on the store in the presence of parent aircraft[8]. The store location for a specified short interval of time is computed by solving the 6-DOF equations of motion by taking into account all external loads acting on the store. The store is automatically set at this computed location and orientation through servo controlled actuators and the loads measured again. The accuracy of the rig is of the order of 0.5mm. in location and 0.1° in orientation. This process is repeated till the store reaches a specified safe distance from the parent aircraft. The complete trajectory of the store can be traced in about one or two blowdowns of 25-30 secs. duration.

The NAL CTS has a dedicated control system interfacing the mechanical and computer hardwares and controlled through the software. A number of hardware as also software safety features and interlocks are provided for the safety of the rig during a tunnel run. Also a provision is built for manual control of the drives, through a pendant. The complete system was successfully commissioned in the year 1990.

Several operational modes are possible with the NAL CTS while the rig is on a trolley outside the tunnel, as well as in the test section. Inside the test section, both grid and trajectory tests are possible. For the present test case trajectory run mode was used to get the regular trajectory of the store separating from the parent aircraft.

Model and Balance Details

Scaled model of store consistent with aircraft model was fabricated. To measure loads on this store, a 6 component strain gauge balance was also designed and fabricated. The store model was mounted on a strut through a small cut-out at the bottom surface boat tail region (Fig. 14). This strut avoids possible errors due to sting interference, base modification and truncation. The correction due to the cavity pressure on the store forces and moments has been taken into account with the measured cavity pressure using a sensitive miniature pressure transducer, at all trajectory points. However, the effect of the strut on the aft end of the model was assumed small which needs verification by experiments.

Typical set up of the store model mounted on the CTS rig kept in the wind-tunnel is shown in Fig. 13. Test results obtained on the store at selected Mach number and incidence, compared against AMAR computations, are discussed below.

Simulated state-histories of full fuel tank released from IFA-1 at M=0.9, α=3.5° are shown in Fig. 15. AMAR computations are compared against CTS data. The states compared are three relative locations X, Y, Z of store c.g. with respect to carriage position, and two Euler angles θ, ψ of store body axes w.r.t. inertial axes. X, Y and Z are positive to rear, starboard and down respectively, while ϕ, θ and ψ are positive right-wing down, nose-up and nose-right. It is seen that the c.g. position transitions compare well, while there are discrepancies in angular states. These differences are to an extent due to the strut on which the store is supported. While the strut resists the cross-flow aft of c.g. at moderate β creating larger pressure difference across the store plane of symmetry and attendent damping of sideslip, the pressure on surface area covered by the strut and its cavity have also to be reliably corrected for. The latter will influence lift and more significantly the pitching moment.

Simulated state histories of empty fuel tank released from IFA-1 at M=0.5, α=3.5° are shown in Fig. 16. Steady aerodynamic predictions are used to obtain trajectories

evaluated at four time step size 'Δt' levels - 0.1, 0.05, 0.025 & 0.01 secs.. It is seen that the computed state trajectories tend to converge with decreasing Δt, and there is little difference between trajectories obtained with Δt= 0.025 and 0.01. Thus for a given separation case, there will be an optimum Δt value at which trajectories are reasonably accurate, and computation time is not unduly high. This optimum Δt value needs to be automatically and dynamically evaluated, i.e. to be 'simulation-adapted'.

Fuzzy-Logic Control of optimum time step size

First the factors that influence the time step size need to be identified. In the absence of thrust, only aerodynamic and inertial (gravitational) forces act on the store after release. Since inertial forces and moments (around c.g.) are invariant with store motion, larger the ratio of inertial to gravitational forces, the larger a Δt one can afford in the simulations. Thus, an optimum Δt has to be inversely proportional to the ratio of lift-to-weight, as may be evaluated at t=0, i.e. at carriage. If the store is aerodynamically stable, errors in prediction, particularly of the angular states, will tend to be damped; conversely errors in these states will tend to amplify if the store is unstable. Thus optimum Δt varies directly with store aerodynamic stability as evaluated under interference free conditions. Both the above factors are 'static', i.e. time-invariant, and hence may be evaluated at the start of simulation.

Optimum Δt can also be inferred to be inversely variant with instantaneous mutation rate of aerodynamic coefficients, since these coefficients serve as transient inputs in the time-marching solution of the equations of motion. Representing the average (weighted - with higher values to C_m and C_n) rate of change of coefficients at a certain time-step as Q(t), $\Delta t(t)$ may be controlled in a classical sense using the simple open-loop transfer function $\Delta t = K/Q$, K being an user-specified constant. Thus there are three inputs, two 'static' and one 'dynamic', and one control output - Δt.

A fuzzy logic control system using triangular membership functions, linguistic rule definitions and centre-of-area defuzzifier[9] is implemented in AMAR code for controlling the optimum time step size. The roles performed by user-specified constants like 'K' above are encapsulated in the definitions of fuzzy associative rules. The effectiveness of control achieved on Δt is checked by comparing the resultant truncation errors of integration at each time step - significant variations with time are damped out.

The trajectory states of the full fuel tank released from IFA-1 at M=0.5, α=3.4° are plotted in Fig. 17. The plots compare both steady and unsteady state evolutions. This is a case where inertial forces dominate over aerodynamics in trajectory determination, even then the dynamic response of the pitch-state is clearly visible - incrementing the store nose pitch-up. The fast downward translation induces a higher incidence angle on the 'dynamic' store due to an upwards shift of the effective velocity vector of the incident flow. The C_N and C_m versus α curve slopes are positive (Figs. 2 & 3), hence the increase in effective α leads to higher C_N and C_m in the unsteady case. The effect of higher lift is not visible on the Z-state evolution due to the predominance of weight, but the angular state θ reflects the higher pitching moment about c.g. as there is no damping inertial moment. To establish the link between dynamic excitation and observed effects on state-histories more methodically, as also to get a quantitative feel for the unsteady effects, a new concept of 'artificial hysteresis' is evolved.

Artificial Hysteresis

An unsteady *oscillatory* solution/test should show the phenomenon of hysteresis — a lag in certain dependent variables as independent parameters occupy identical values but in reverse motion. The steady solution at the same values of independent parameters should be close to mean of the two unsteady solutions obtained in opposite directions. Now the separating store represents a 'plunging' motion and hence there is no natural hysteresis. An artificial hysteresis is attemptedly imparted to the store by forcibly reversing its direction of evolution of states at a certain time instant T'. Before T' is reached the store executes its normal forward unsteady evolution, where its state-vector is stored at every time instant. After T' the store is put in 'reverse unsteady evolution' where it simply reoccupies the earlier states at every time instant (i.e. while time t increases continually $|t-T'|$ is reflected and used for selection of corresponding stored state vector) and 6-DOF equations are redundant. The unsteady CFD solution is recomputed at each of these reverse time-instants. The difference between the forward and reverse unsteady CFD solutions is the focus of interest.

Using artificial hysteresis one would expect to observe the following from the C_N, C_m, C_S and C_n vs. t curves -

i) There should be a consistent 'gap' - as opposed to criss-crossing - between the forward and reverse computed values of above coefficients and this gap should approach 0 as $t \rightarrow 0$
ii) The steady evolutionary solutions should 'approximately' bisect the two opposing unsteady solutions - 'approximate' because in the course of steady evolution the store states occupy slightly different values from those obtained in the unsteady evolution, and these Δ-states grow with time
iii) The difference between coefficient values obtained in the forward and reverse unsteady solutions at any time instant is twice of the 'increment due to unsteadiness' at that instant. This gives a measure of the magnitude and direction of the unsteady increment.

Figure 18 shows artificial hysteresis curves of C_N and C_m for the store separation case depicted in Fig. 17. C_N and C_m are positive upwards and nose up. Features (i) and (ii) above, that may be considered as necessary conditions for correctness of unsteady solutions, are satisfied here. The C_m curve shows a positive increment due to unsteadiness - for the reasons elucidated above - causing the dynamic pitch-up. For the same reason there is a large additional C_N in the unsteady case - which, for stated reasons, is not reflected in the trajectory.

Having used the tool of artificial hysteresis to analyze the dynamics of a translation-dominated moving body, the dynamics of a predominantly rotating body is

investigated next. The empty fuel-tank on IFA-1 at M=0.5, α=3.5° is allowed to rotate freely about its c.g., at carriage, without any relative translation. Thus X, Y and Z are constant with t. Figures 19 and 20 show the evolution of yaw state and the corresponding artificial hysteresis curves for this case. The yaw state is considered since it is the predominant direction of rotation and there is no significant change in aircraft interference intensity across this movement. It is seen that the unsteady effects seem to amplify the yawing motion.

To investigate this further, one may express a generic moment coefficient C_a (C_m or C_n) in terms of the angle γ (either α or β) and time t linearly as

$$C_a = k_1\gamma + k_2 t \qquad \text{(i)}$$

where k_1 and k_2 are constants. Now

$$\partial C_a/\partial\gamma = k_1 + k_2\,(\partial t/\partial\gamma)$$

and $\partial t/\partial\gamma$ is instantaneously zero for steady flow (as is $\partial\gamma/\partial t$), so that

$$\partial C_a/\partial\gamma = k_1 \qquad \text{(ii)}$$

in steady case. Obviously, k_1 is <, > 0 in stable and unstable cases of configuration aerodynamics. Also,

$$\partial C_a/\partial t = k_1\,(\partial\gamma/\partial t) + k_2 \qquad \text{(iii)}$$

It follows that $k_2 = \partial C_a/\partial t$ in the steady case, and from (ii) and (iii) one can write

$$\partial C_a/\partial t = \text{steady } C_a \text{ vs. t slope} + k_1\,(\partial\gamma/\partial t),$$

i.e. $k_1(\partial\gamma/\partial t)$ is the unsteady increment to C_a vs. t slope.

If $\partial\gamma/\partial t$ is positive, (as is currently in forward evolution - Fig. 19), then —

for stable case ($k_1 < 0$), $\partial C_a/\partial t <$ the steady slope,

for unstable case ($k_1 > 0$), $\partial C_a/\partial t >$ steady slope,

if $\partial\gamma/\partial t$ is negative, (as in current reverse evolution) —

for stable case, $\partial C_a/\partial t >$ steady slope

for unstable case, $\partial C_a/\partial t <$ steady slope

From the steady curves in Figs. 19 and 20, it is seen that the store is unstable in yaw (C_n increases with ψ). The consequent inequalities that follow from the above relations are faithfully reflected in the artificial hysteresis curves in Fig. 20. It may also be verified that the artificial hysteresis evaluations quantitatively capture unsteady increments in $\partial C_a/\partial t$ as predicted by Eq. (iii) using values of k_1 and k_2 obtained from steady case. For example, at t=0.15, Eq. (iii) predicts a value of 2.579 for the time derivative of C_n in forward unsteady evolution (the steady evolution slope is 1.186), while the computed value from actual unsteady solution is 2.498. This demonstrates the usefulness of the tool of artificial hysteresis to not only isolate and measure unsteady effects, but to validate correctness of unsteady solution, of course within linear range of angular states.

Aerodynamic computations using FIM code alone were performed on an indigenous parallel super-computer PACE+, while on-line trajectory simulations using the synergized AMAR code were executed sequentially on Indigo workstations with R10000-chip processors, where each simulation case took 12 to 20 hours of computation time.

Conclusions

The hybrid integral-equation finite-volume approach to solution of fluid flows can 'naturally' handle arbitrarily complex configurations, including those with components in relative motion, as typical of separating stores.

The FIM code based on above approach is extended to unsteady flows.

The technique of *artificial hysteresis* is established for analyzing dynamic effects of non-oscillatory motion.

Fuzzy logic control of optimum time step size for maximum simulation accuracy in minimum computation time is implemented.

An efficient technique for aerodynamic accuracy accretization by incorporation of real-flow effects on inviscid computations, using what may be termed as 'accuracy-interference increment parallelogram', is also developed.

Comparisons of AMAR trajectory simulations against preliminary CTS results are encouraging.

Acknowledgment

The authors acknowledge support of their parent organizations, ADA and NAL, to this task. They are specially thankful to Dr. Kota Harinarayana, Program Director, Dr. T.S. Prahlad, NAL Director, Dr. T.G. Pai, Project Director (Technology Development) and Dr. K.P. Singh, Group Director (CFD) for their support and encouragement. Many thanks are also due to the staff of NAL WT Centre, particularly to Mr. Rajan Kumar, Mr. V. Kamaraj and Mr. G. Narayan.

References

1. Bhattacharya, A.K. and Arora, N.L., "A Hybrid Integral Equation Finite Volume scheme for Transonic Potential flow over Complex Configurations", Aeronautical Journal, Feb. 1994, pp. 34-48.
2. Bhattacharya, A.K. and Arora, N.L., "A Field Integral technique for Leading Edge Separated flow over delta wings at Transonic speeds", *Proceedings of 6th International Symposium on CFD*, Lake Tahoe, USA, Sep. 1995, pp. 105-110.
3. Bhattacharya, A.K., "Unsteady Transonic Integral Equation scheme for Trajectory Simulation of Stores", AIAA Paper, 98-0751.
4. Keen, K.S., "New approaches to computational aircraft/store weapons integration", AIAA Paper, 90-0274.
5. Dillenius, M.F.E., Stanley, C.P. and Nixon, N., "Pylon Carriage and Separation of Stores", *Progress in Aeronautics and Astronautics*, Vol. 141, Chap. 13, 1992, pp. 575-666.
6. Sellars, N.D. and Hall, I.M., "An evaluation of advanced CFD codes for stores at incidence", Paper No. 6 in *Aerodynamics of store integration and separation*, AGARD-CP-570, Feb. 1996.
7. Bhattacharya, A.K., "Analysis of Store Aerodynamics in varying proximity to aircraft, using Wind Tunnel and CFD data", ADA Rep. No. TD/010601/069, Sep. 1996.
8. Kanagarajan, V., Kamaraj, V., Rajan Kumar and Santhakumari, S., "Measurement of Carriage Loads on Wing mounted External Stores", Journal of Aeronautical Society of India, Feb. 1997, pp. 8-14.
9. Kosko, B., *Neural Networks and Fuzzy Systems*, Englewood Cliffs, NJ, Prentice Hall, 1992.

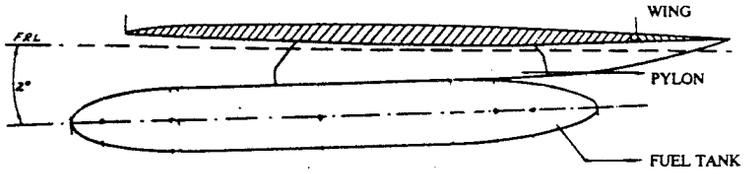

Fig. 1. Schematic of Fuel Tank in Carriage position

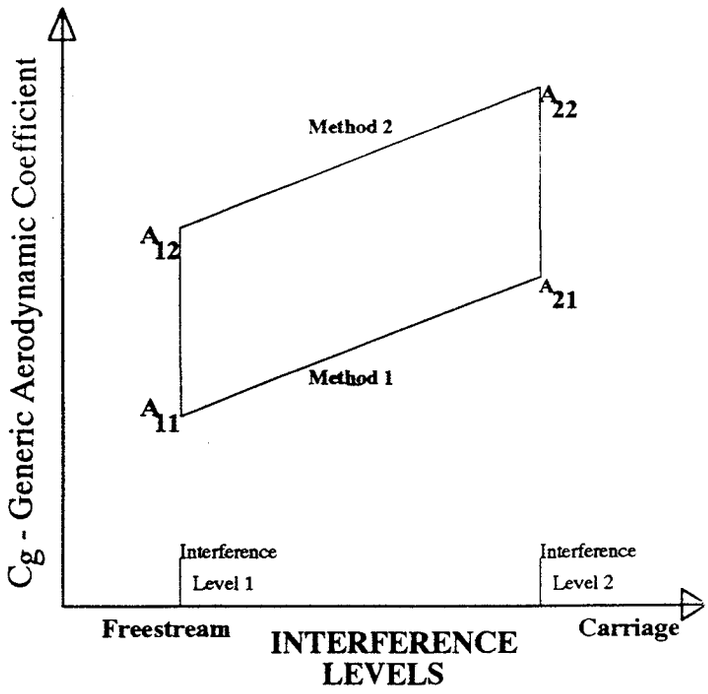

Fig. 4. Conceptual Parallelogram of Accuracy- and Interference- Increments

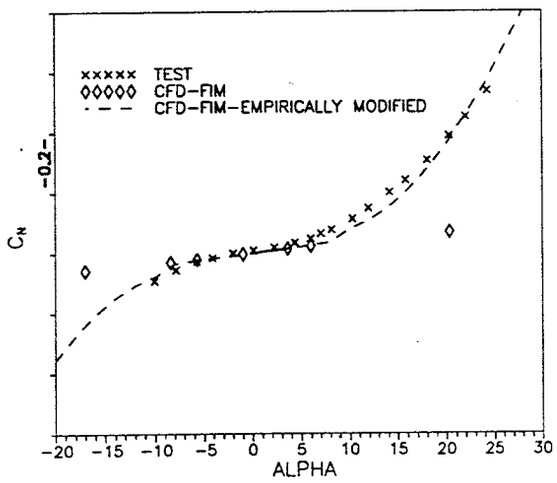

FIG.2 : C_N vs. ALPHA ON FUEL TANK IN FREESTREAM AT M=0.9

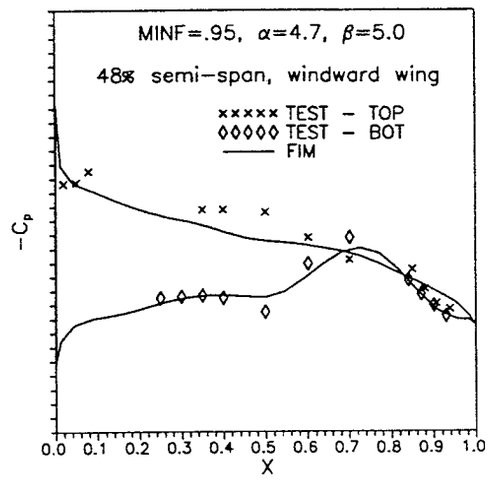

Fig. 5: PRESSURE DISTRIBUTION ON AIRCRAFT WING

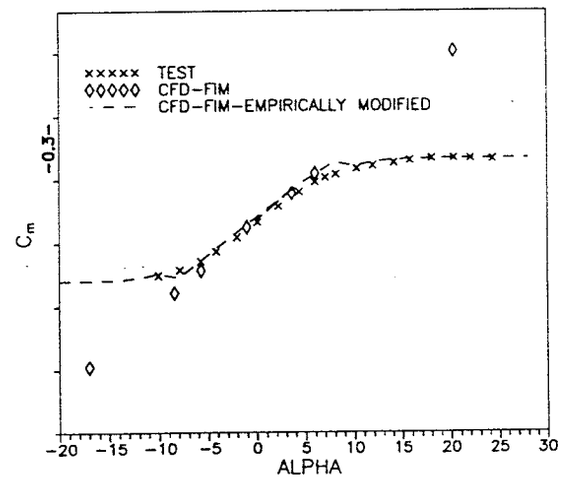

FIG.3 : C_m vs. ALPHA ON FUEL TANK IN FREESTREAM AT M=0.9

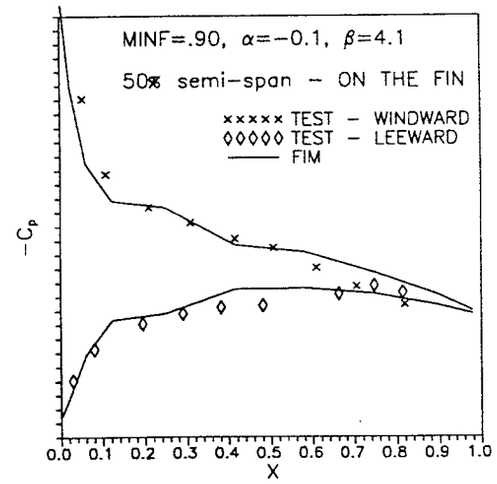

Fig. 6: PRESSURE DISTRIBUTION ON VERTICAL FIN

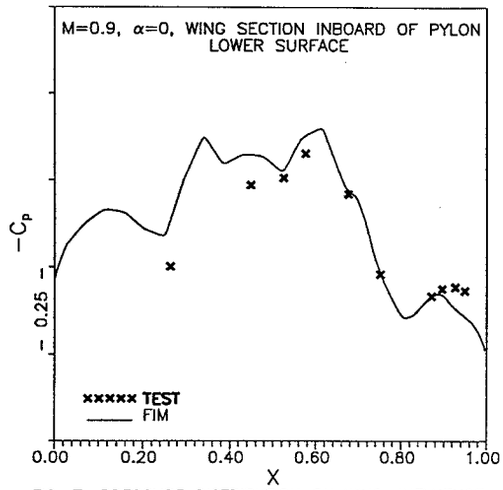

FIG. 7: PRESSURE DISTRIBUTION ON WING, INFLUENCE OF STORE CARRIAGE ON INBOARD SECTION – STRONG SHOCK FORMATION AT M=0.9, α=0

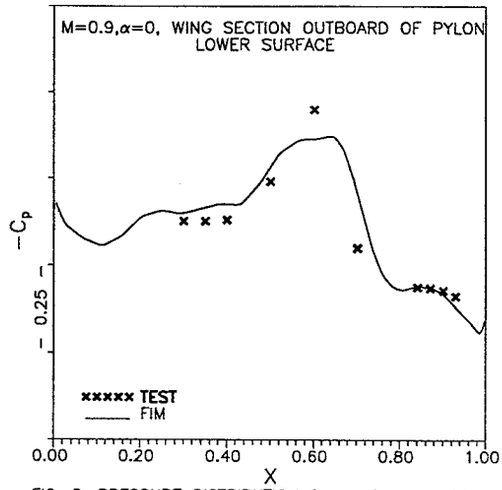

FIG. 8: PRESSURE DISTRIBUTION ON WING, INFLUENCE OF STORE CARRIAGE ON OUTBOARD SECTION – STRONG SHOCK FORMATION AT M=0.9, α=0

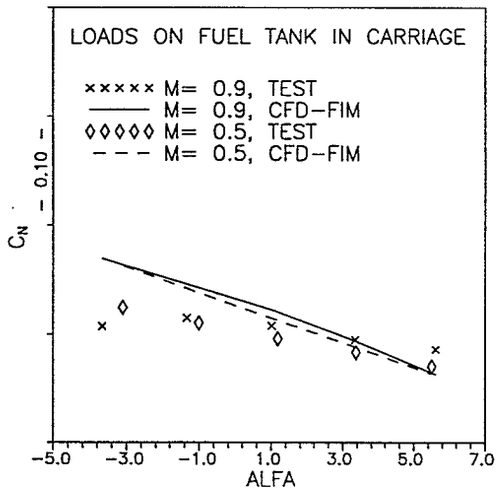

FIG. 9. C_N vs. α, FUEL TANK IN CARRIAGE

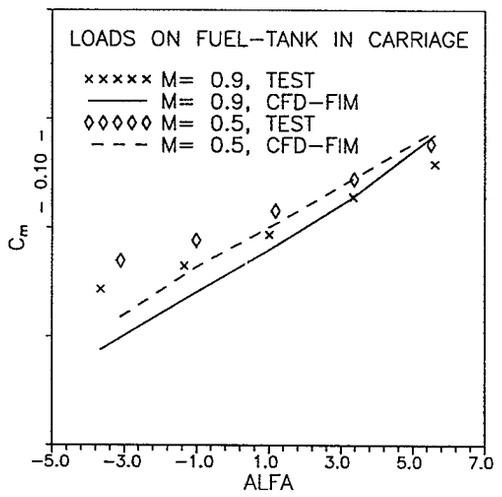

FIG. 10. C_m vs. α, FUEL TANK IN CARRIAGE

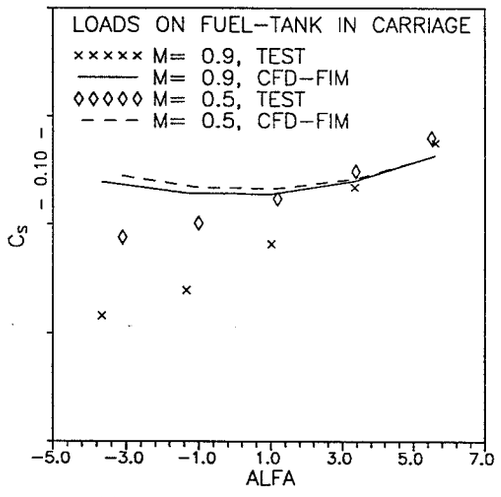

FIG. 11. C_S vs. α, FUEL TANK IN CARRIAGE

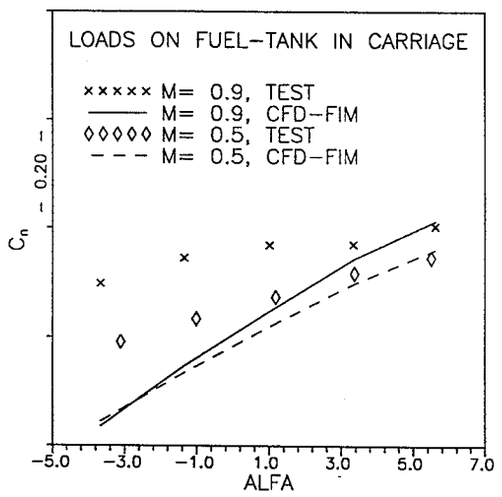

FIG. 12. C_n vs. α, FUEL TANK IN CARRIAGE

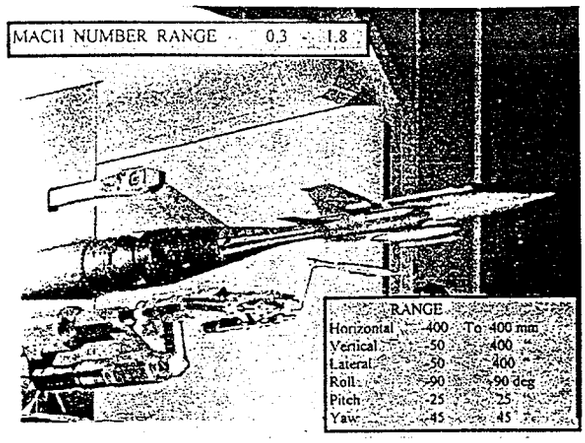

Fig. 13. Typical test setup of CTS in NAL 1.2m Tunnel

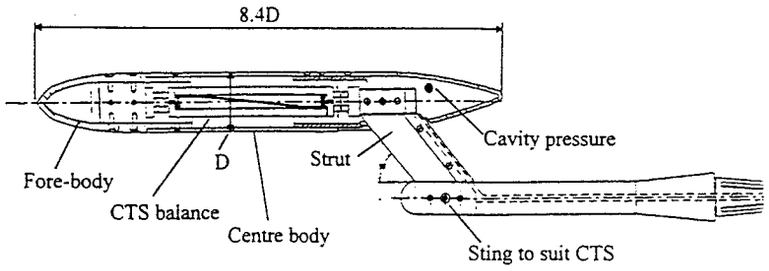

Fig. 14. Assembly of Store Model - CTS Balance

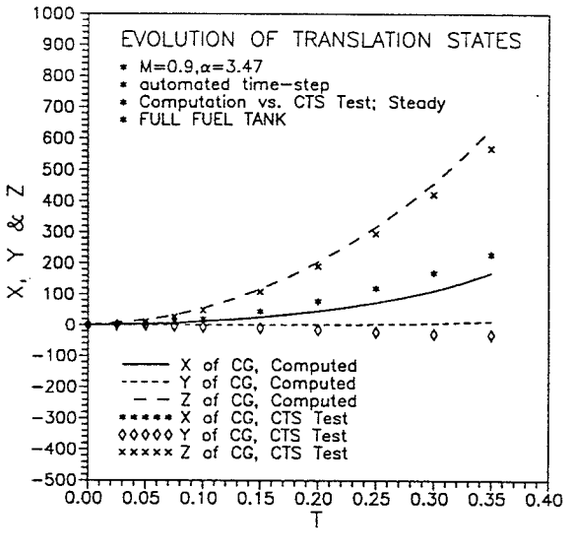

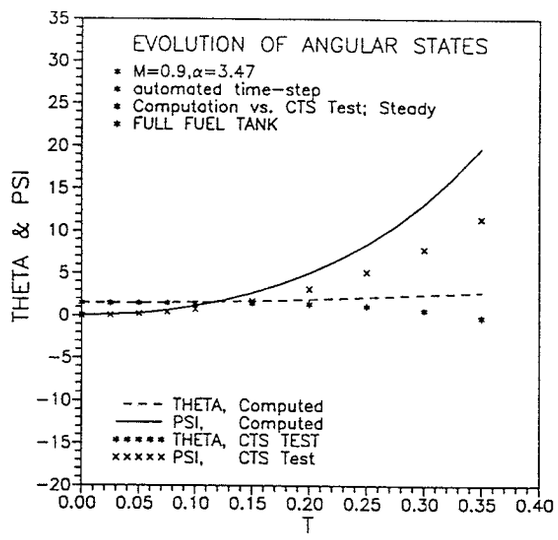

FIG. 15. TRAJECTORY EVOLUTION OF FUEL TANK, FULL, AT M=0.9,α=3.47, AMAR COMPUTATION vs. CTS TEST

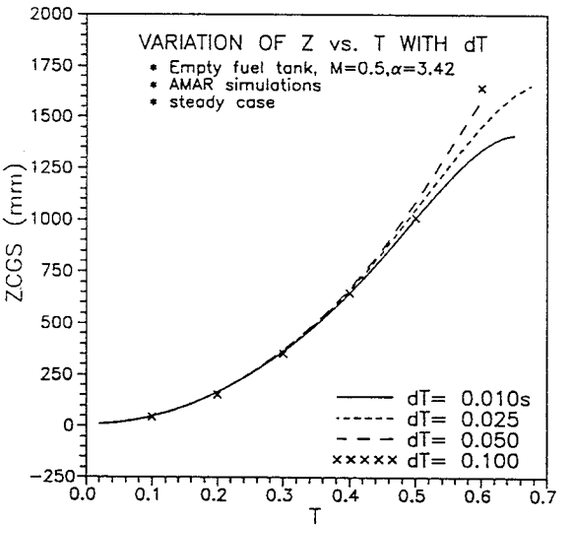

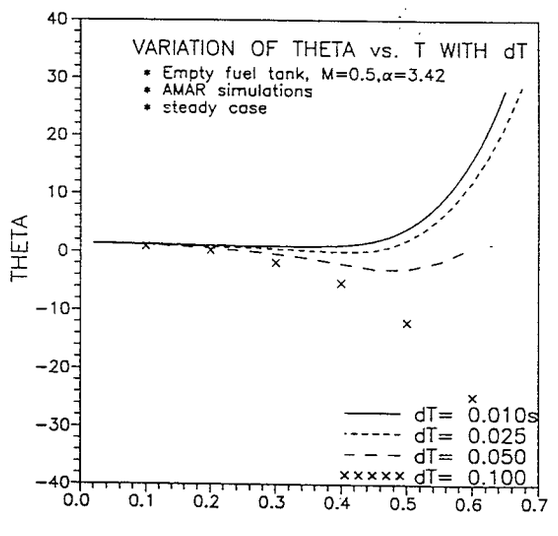

FIG. 16. VARIATION OF STATE-HISTORIES WITH TIME STEP SIZE dT IN AMAR SIMULATIONS

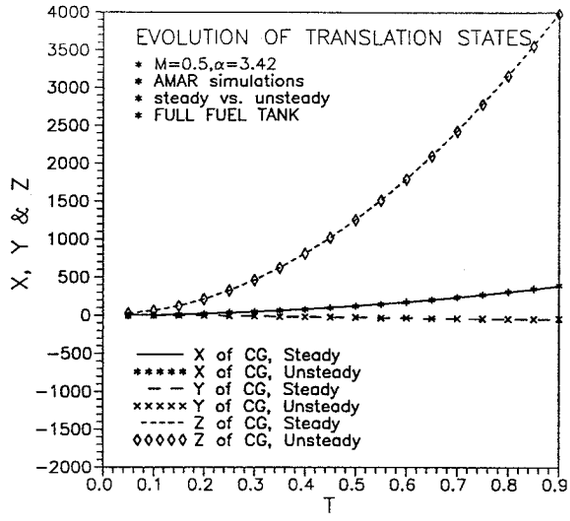

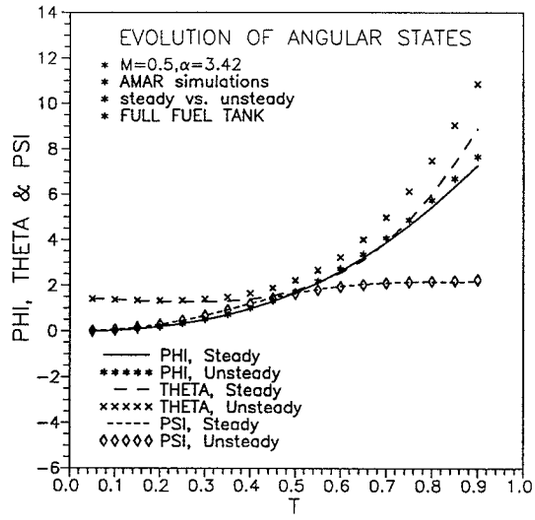

FIG. 17. TRAJECTORY EVOLUTION OF FUEL TANK, FULL, AT M=0.5,α=3.42, STEADY vs. UNSTEADY COMPUTATION

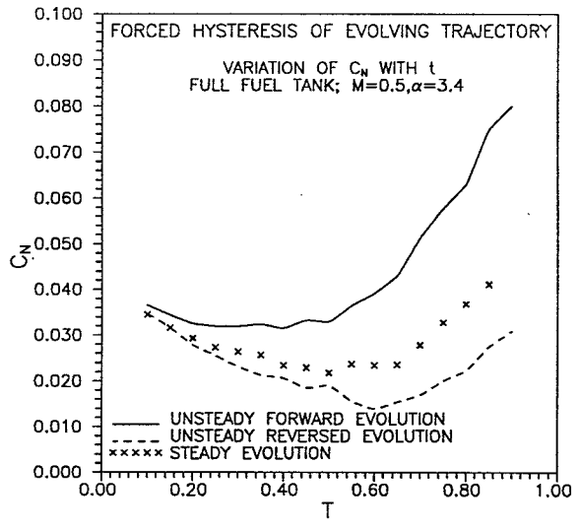

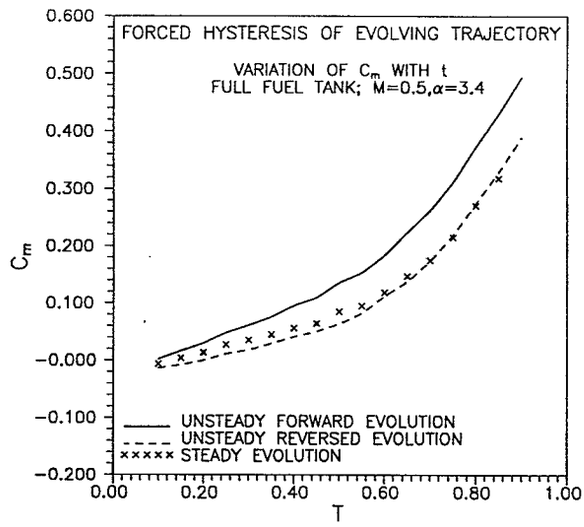

FIG. 18. ARTIFICIAL HYSTERESIS BY FORCED INVERSION OF TRAJECTORY EVOLUTION, FULL FUEL TANK

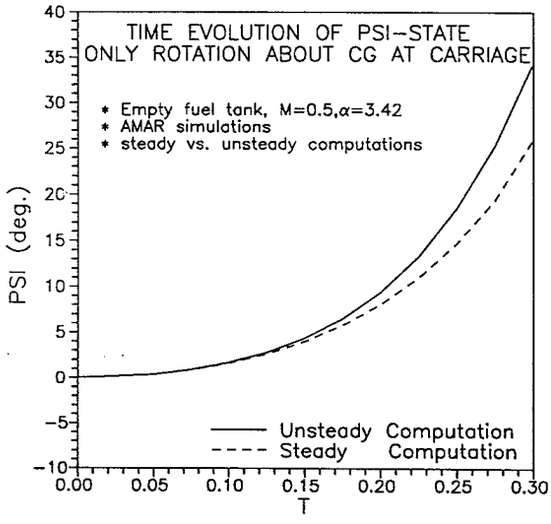

FIG. 19. Evolution of PSI-state with time, store free only to rotate about c.g. at carriage

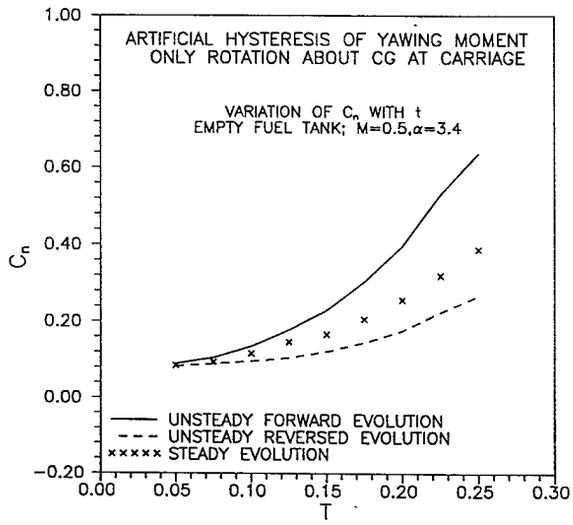

FIG. 20. Artificial Hysteresis by forced inversion of evolving trajectory, empty fuel tank